

Reduced cross-section in Electron-Ion Colliders at small x

G.R.Boroun* and B.Rezaei†

Department of Physics, Razi University, Kermanshah 67149, Iran

(Dated: April 22, 2024)

The nuclear reduced cross section σ_r^A , in the kinematic range of the electron-Ion collider with center-of-mass energy $\sqrt{s} = 140$ GeV and $y \leq 1$, is discussed. The importance of the nuclear longitudinal structure function F_L^A and its behavior owing to the impact parameter for the heavy and light nucleus of Pb-208 and C-12 at $Q^2 = 5$ and 10 GeV² is considered. The dependence of the ratios $R_{F_L}^A$ and R_σ^A on the impact parameter and the expanding point of the gluon density at small x are investigated. The factorized form of parton distributions in nuclei is used in HIJING2.0 model.

I. Introduction

The shadowing seen [1] in nuclear deep inelastic scattering (DIS) at small Bjorken x (where x is the longitudinal momentum fraction of the nucleon carried by the struck parton) is a distinct phenomenon when the nuclear structure functions compared to that for free nucleons. The DIS of leptons off nuclei offers a unique opportunity for the detailed mapping of nuclear structure in the wide range of x and Q^2 (where Q^2 the (negative) boson virtuality exchanged between the lepton and the quark from the nucleus). The shadowing at small x states that the structure function per nucleon is smaller in nuclei than in a free nucleon and characterized by depletion of F_2^A with respect to F_2^p [2-4].

Nuclear structure functions (F_2^A and F_L^A) are needed in the computation of reduced cross section in high energy nuclear collisions. In the framework of DIS, it is possible to extract the nuclear structure functions from the singlet and gluon distribution functions as parameterized in Refs.[5,6]. These parameterizations describe very well the available experimental data of the reduced cross section. They provide a behavior of the cross sections $\sim \ln^2 1/x$, in an agreement with the Froissart predictions [7]. These results for the longitudinal structure function have been reported in Refs.[8-11], where the longitudinal structure function extracted at moderate and low values of x is in reasonably good agreement with the available experimental data.

The nuclear reduced cross section σ_r^A can be standardly defined via the structure functions F_2^A and F_L^A for the collision of the transversal and longitudinal virtual photon of momentum q , $q^2 = -Q^2$, on the nucleus A by

$$\sigma_r^A(x, Q^2) = F_2^A(x, Q^2) - \frac{y^2}{Y_+} F_L^A(x, Q^2), \quad (1)$$

where $Y_+ = 1 + (1 - y)^2$ with the inelasticity variable y . The nuclear structure function of a nuclei A with Z protons and N=A-Z neutrons is

$$F_2^A(x, Q^2) = \sum_q e_q^2 \left[x f_q^{p/A}(x, Q^2) + x f_{\bar{q}}^{p/A}(x, Q^2) \right], \quad (2)$$

where the nuclear parton distribution functions (nPDFs) read

$$f_i^A(x, Q^2) = \frac{Z}{A} f_i^{p/A}(x, Q^2) + \frac{N}{A} f_i^{n/A}(x, Q^2), \quad (3)$$

and $f_i^{p/A}$ and $f_i^{n/A}$ are the parton distribution functions (PDFs) of a bound proton and neutron in a nuclei A respectively. Nuclear effects in the nPDF and in the structure function F_2^A are defined by the following forms

$$\begin{aligned} R_i^A(x) &= \frac{x f_i^A(x, Q^2)}{A x f_i^p(x, Q^2)}, \\ R_{F_2}^A(x) &= \frac{F_2^A(x, Q^2)}{A F_2^p(x, Q^2)}, \end{aligned} \quad (4)$$

which is defined by small x shadowing [12]. The different perturbative QCD-based models at scales relevant to LHC and RHIC experiments for nuclear shadowing of gluons have been investigated in Ref.[13]. The shadowing of gluons is defined by

$$R_G^A(x) = \frac{x g^A(x, Q^2)}{A x g^p(x, Q^2)}. \quad (5)$$

This phenomenon is defined as a recombination effect at small x due to high gluon number density in the Infinite Momentum Frame (IMF) where nucleus is fast. The behavior of the small x gluons from different nucleons leads to depletion of the nuclear density, which is referred to as saturation of gluon density. This slows down the unlimited growth of the gluon distribution function. The shadowing seen in nuclear DIS [14] for $x \leq 0.01$ is characterized by comparison of the nuclear structure function with the proton structure function. Within the color glass condensate (CGC) saturation approach [15], this effect predicted a saturation scale $Q_s(x)$

*Electronic address: boroun@razi.ac.ir

†brezaei@razi.ac.ir

which establishes the region where the increasing of the unintegrated gluon distribution (UGD) on x is tamed. In the simplest form, the saturation scale is estimate to be $Q_{s,A}^2 \propto A^{\frac{1}{3}}$. Saturation effect at small x will be one of the key physics goals of an Electron-Ion Collider (EIC) [16,17]. This construction, with a possibility to operate with a wide variety of nuclei, will extend the kinematic acceptance to x and Q^2 with varying center-of-mass energies from $\sqrt{s} = 20 - 140$ GeV and $0.01 \leq y \leq 0.95$ which is very important to effectively constrain nPDFs [18,19]. The interactions in the EIC will be probes regions of progressively higher gluon density in nuclei.

The purpose of this paper is to evaluate the nuclear reduced cross section in the kinematic regions corresponding to the EIC for eA collision. We produce results for the F_2^A and F_L^A using the parametrization method [5,6] owing to the adopted x dependence of the ratio of structure functions.

The structure of the manuscript is as follows. In Section II we review the method to compute the nuclear reduced cross section as the virtual photon-nucleus cross section is smaller than A times the photon-nucleon cross section. Results for the parametrization of the proton structure functions are shown and discussed in Section III. Finally, we present our results and conclusions in Section IV.

II. γ^* -A scattering

The reduced cross section for electron scattering from a nucleus directly is dependent on the double differential cross section as

$$\sigma_r^A \equiv \left(\frac{d^2 \sigma^{lA}}{dx dQ^2} \right) \frac{x Q^4}{2\pi \alpha_{em}^2 [1 + (1-y)^2]}, \quad (6)$$

where $\frac{d^2 \sigma^{lA}}{dx dQ^2}$ is dependent on the lepton and nucleus tensors [4,12,20]. The deeply inelastic lepton-nucleus scattering (DIS) experiments are the cleanest way of getting information of the nPDF. The nuclear tensor $W_{\mu\nu}^A$ is defined by the nucleon tensor as

$$W_{\mu\nu}^A(p_A, q) = \int d^4 p_N S(p_N) W_{\mu\nu}^N(p_N, q), \quad (7)$$

where $p_{A,N}$ are the nuclear and nucleon momentums respectively, and the spectral function $S(p_N)$ is the nucleon momentum distribution in a nucleus. The nuclear transverse and longitudinal structure functions are defined in terms of the structure functions W_1^A and W_2^A where they are in accordance with the photon polarization vectors¹

[21]. In the nucleus rest frame they are defined by²

$$\begin{aligned} F_1^A(x_A, Q^2) &= \sqrt{p_A^2} W_1^A(p_A, q), \\ F_2^A(x_A, Q^2) &= \frac{p_A \cdot q}{\sqrt{p_A^2}} W_2^A(p_A, q), \end{aligned} \quad (8)$$

where $x_A = \frac{M_N}{M_A} x$ and the longitudinal nuclear structure function reads

$$F_L^A(x_A, Q^2) = \left(1 + \frac{Q^2}{\nu^2} \right) F_2^A(x_A, Q^2) - 2x_A F_1^A(x_A, Q^2). \quad (9)$$

The nuclear structure function F_2^A is the structure function F_2 for a nuclear target A which can be standardly defined via the cross sections $\sigma_{T,L}$ for the collision of the transversal (T) or longitudinal (L) virtual photon on the nucleus A as

$$F_2^A(x, Q^2) = \frac{Q^2}{4\pi^2 \alpha_{em}} (\sigma_T^{\gamma^* A} + \sigma_L^{\gamma^* A})(x, Q^2). \quad (10)$$

Over a wide saturation kinematic range (i.e., $10^{-5} \leq x \leq 0.1$ and $0.05 \leq Q^2 \leq 100$ GeV²), reduction of the nuclear reduced cross section with respect to the σ_r^p is given by

$$R_\sigma^A(x) \equiv \frac{\sigma_r^A(x, Q^2)}{A \sigma_r^p(x, Q^2)} = \frac{F_2^A(x, Q^2) - \frac{y^2}{Y_+} F_L^A(x, Q^2)}{A \left[F_2^p(x, Q^2) - \frac{y^2}{Y_+} F_L^p(x, Q^2) \right]}, \quad (11)$$

where the behavior of the longitudinal structure functions is dependent on the gluon distribution at small x . The longitudinal structure function according to the Altarelli-Martinelli [22] equation in QCD at small x using the expansion method [23] for the gluon distribution function at an arbitrary point $z = a$ has been obtained at the leading-order (LO) approximation in Ref.[24] by the following form³

$$F_L^A(x, Q^2) \simeq \frac{10\alpha_s}{27\pi} x g^A \left(\frac{x}{1-a} \left(\frac{3}{2} - a \right), Q^2 \right). \quad (12)$$

The normalized ratio of the longitudinal structure function is defined

$$R_{FL}^A(x) = \frac{F_L^A(x, Q^2)}{A F_L^p(x, Q^2)} \simeq R_G^A(kx), \quad (13)$$

where $k = \frac{3-2a}{2-2a}$. Therefore, the ratio R_σ^A at small x can be approximately expressed in terms of the proton

¹ The polarization vectors for the virtual photon are defined by $\epsilon_\pm = \mp(0, 1, \pm i, 0)/\sqrt{2}$ and $\epsilon_0 = \mp(\sqrt{\nu^2 + Q^2}, 0, 0, \nu)/\sqrt{Q^2}$ where ν is the energy transfer $\nu = E_e - E'_e$.

² For future discussion, please refer to Ref.[21].

³ At small x the gluon distribution is the dominant one in the longitudinal structure function.

structure functions as

$$R_\sigma^A = \frac{F_2^A(x, Q^2) - \frac{y^2}{Y_+} F_L^A(x, Q^2)}{A \left[F_2^p(x, Q^2) - \frac{y^2}{Y_+} F_L^p(x, Q^2) \right]} \quad (14)$$

$$\simeq \frac{R_{F_2}^A(x) F_2^p(x, Q^2) - \frac{y^2}{Y_+} \frac{10\alpha_s}{27\pi} R_G^A(kx) x g^p(kx, Q^2)}{F_2^p(x, Q^2) - \frac{y^2}{Y_+} \frac{10\alpha_s}{27\pi} x g^p(kx, Q^2)}.$$

In the following, we discuss the parametrization for the nuclear parton distributions into the parametrization of $F_2^p(x, Q^2)$, $F_L^p(x, Q^2)$ and $xg^p(x, Q^2)$ [5-11].

III. Structure Functions

At small values of the Bjorken variable x , the parametrization of $F_2^p(x, Q^2)$ is presented based on an accurate fit to the HERA data for $Q^2 \geq 0.15 \text{ GeV}^2$ in Ref.[5]. This parametrization by the form

$$F_2^p(x, Q^2) = D(Q^2)(1-x)^n \sum_{m=0}^2 A_m(Q^2) L^m, \quad (15)$$

describes fairly well the available experimental data on the reduced cross sections, and it is pertinent in investigations of the scattering of cosmic neutrinos from hadrons. The effective parameters read

$$\begin{aligned} D(Q^2) &= \frac{Q^2(Q^2 + \lambda M^2)}{(Q^2 + M^2)^2}, \\ A_0(Q^2) &= a_{00} + a_{01} L_2(Q^2), \\ A_i(Q^2) &= \sum_{k=0}^2 a_{ik} L_2(Q^2)^k, \quad i = (1, 2), \\ L(Q^2) &= \ln \frac{1}{x} + \ln \frac{Q^2}{Q^2 + \mu^2}, \\ L_2(Q^2) &= \ln \frac{Q^2 + \mu^2}{\mu^2}, \end{aligned} \quad (16)$$

where, the coefficients are defined in Table I.

An analytical derivation of the gluon distribution function from the known structure function $F_2^p(x, Q^2)$ (i.e., Eq.(15)) and its derivative $\frac{dF_2^p(x, Q^2)}{d \ln Q^2}$ to include the effects of heavy-quark masses based on Laplace transforms is extended in Refs.[25, 6]. The gluon distribution function is derived directly using a Laplace transform method, for four massless quarks, by the following form

$$\begin{aligned} xg(x, Q^2) &= \frac{9\pi}{5\alpha_s} \left\{ 3F_2^p(x, Q^2) - x \frac{\partial}{\partial x} F_2^p(x, Q^2) \right. \\ &\quad - \int_x^1 F_2^p(z, Q^2) \left(\frac{x}{z} \right)^{3/2} \left[\frac{6}{\sqrt{7}} \sin\left(\frac{\sqrt{7}}{2} \ln \frac{z}{x}\right) \right. \\ &\quad \left. \left. + 2 \cos\left(\frac{\sqrt{7}}{2} \ln \frac{z}{x}\right) \right] \frac{dz}{z} \right\}, \end{aligned} \quad (17)$$

where

$$\mathcal{F}_2^p(x, Q^2) = \frac{\partial F_2^p(x, Q^2)}{\partial \ln Q^2} - \frac{\alpha_s}{4\pi} \left\{ \int_x^1 \frac{\partial F_2^p(z, Q^2)}{\partial z} \times \left[\frac{16}{3} \ln \frac{z}{z-x} - \frac{4}{3} \left(\frac{x^2}{z^2} + \frac{2x}{z} \right) \right] dz \right\}. \quad (18)$$

Here α_s is the running coupling at the LO approximation with $\alpha_s(M_z^2) = 0.118$ and $\Lambda_{n_f=4} = 120.4 \text{ MeV}$ and $\Lambda_{n_f=5} = 87.8 \text{ MeV}$. Similar investigations of the longitudinal structure function, with respect to the Mellin and Laplace transform methods, have been performed in Refs.[8,10,26].

Parameterizations of the nuclear parton distribution functions proposed by some groups such as Eskola, Kolhinen and Salgado (EKS) [27], by de Florian and Sassot (DS) [28], by Hirai, S. Kumano and T. H. Nagai (HKN) [29], by K. J. Eskola, H. Paukkunen and C. A. Salgado (EPS) [30] and briefly discussed in Refs.[31-33] respectively. Some recent works determined the nuclear partons in Refs.[34-37]. In Ref.[34], the new nCETQ15 extends CTEQ proton PDFs to include the nuclear dependence using data on nuclei all the way up to ^{208}Pb with uncertainties using the Hessian method. An updated global analysis of collinearly factorized nuclear parton distribution functions (nPDFs) at next-to-leading order approximation (NLO) in perturbative QCD is presented in Ref.[35] which includes more data from proton-lead collisions at the Large Hadron Collider (LHC). The shadowing and anti-shadowing effects on gluons in large nuclei are considered at small and intermediate values of x . The uncertainties of nPDFs are included within the Hessian framework. Global NLO QCD analysis of hard processes in fixed-target lepton-nucleus and proton-nucleus together with collider proton-nucleus experiments are presented in Ref.[36] for determination of nuclear parton distributions and provide predictions for ultra-high-energy neutrino-nucleon cross-sections, relevant for data interpretation at neutrino observatories. The extensive dataset underlying the nNNPDF3.0 determines the shadowing of gluons and sea quarks as well as the anti-shadowing of gluons at small and large x values respectively.

In the following, the HIJING [37,38] parametrization is considered, which is in good agreement with the ALICE experiment at LHC energies, which provides a more stringent constraint on gluon shadowing. The nuclear modification factors in the HIJING parametrization are given by

$$\begin{aligned} R_{F_2}^A(x, b) &= 1 + 1.19(\ln A)^{1/6} (x^3 - 1.2x^2 + 0.21x) \\ &\quad - s_q(b)(A^{1/3} - 1)^{0.6} (1 - 3.5\sqrt{x}) \\ &\quad \times \exp(-x^2/0.01), \end{aligned} \quad (19)$$

and

$$R_G^A(x, b) = 1 + 1.19(\ln A)^{1/6}(x^3 - 1.2x^2 + 0.21x) - s_g(b)(A^{1/3} - 1)^{0.6}(1 - 1.5x^{0.35}) \times \exp(-x^2/0.004), \quad (20)$$

where $s_a(b)$ reads

$$s_a(b) = s_a \frac{5}{3}(1 - b^2/R_A^2), \quad (21)$$

with $s_q = 0.1$ and $s_g = 0.22 - 0.23$. Indeed, the impact parameter dependence of the shadowing is implemented through the parameters $s_a(b)$ in Eq.(21) of the HIJING2.0 model. The authors, in Ref.[38], defined that the form of the impact parameter dependence is chosen to give rise to the centrality dependence of the pseudorapidity multiplicity density per participant pair. Considering the dependence of the gluon density on the impact parameter, shows that this is stronger than the typical nuclear length $L_A = \sqrt{R_A^2 - b^2}$ dependence.

For a nuclear target with the mass number A , we take $R_A = 1.25 \text{ fm} \times A^{1/3}$ which is the nuclear size. The impact parameter of b is chosen for the central with $b = 0$ and the peripheral with $b = 5 \text{ fm}$ (for heavy nuclei) [4]. Therefore, the nuclear structure functions can be defined and parametrized via the HIJING and F_2^p parametrizations as we find that

$$F_2^A(x, Q^2, b) = AF_2^p(x, Q^2) \text{ (i.e., Eq.15)} \times R_{F_2}^A(x, b) \text{ (i.e., Eq.19)}, \quad (22)$$

and

$$F_L^A(x, Q^2, b) = A \frac{10\alpha_s}{27\pi} xg^p(kx, Q^2) \text{ (i.e., Eq.17)} \times R_G^A(kx, b) \text{ (i.e., Eq.20)}. \quad (23)$$

So, the nuclear reduced cross section is parametrized by the following form

$$\sigma_r^A(x, Q^2, b) = AF_2^p(x, Q^2)R_{F_2}^A(x, b) - \frac{y^2}{Y_+} A \frac{10\alpha_s}{27\pi} \times xg^p(kx, Q^2)R_G^A(kx, b). \quad (24)$$

In the following, the nuclear structure functions, F_2^A, F_L^A and the nuclear reduced cross section, σ_r^A , are determined owing to the EIC data range.

IV. Results and Conclusions

The kinematic regions at the EIC are proposed with $\sqrt{s} = 140 \text{ GeV}$ where the numerical results are determined by inelasticity $y \lesssim 1$. The impact parameter b is selected to be $b = 0$ and 5 fm for heavy nuclei (i.e., Pb-208) and $b = 0$ for light nuclei (i.e., C-12). The

gluon density is expanded when the points $a = 0$ and 0.9 are used. The results for the ratios $R_{F_L}^A$ and $R_{\sigma_r}^A$ and the nuclear structure functions, F_2^A and F_L^A and the nuclear reduced cross section σ_r^A are obtained at scales $Q^2 = 5 \text{ GeV}^2$ and 10 GeV^2 for the nucleus of Pb-208 and C-12 in Figs.1-4 respectively. The ratio of gluon and singlet distributions are used from the HIJING parameterization. In these figures (in the left panels), the ratios $R_{F_2}^A$ (HIJING parametrization, Eq.(19)), $R_{F_L}^A$ (Eq.(13)) and $R_{\sigma_r}^A$ (Eq.(14)) are shown for lead (Pb-208) at $Q^2 = 5 \text{ GeV}^2$ (Fig.1) and $Q^2 = 10 \text{ GeV}^2$ (Fig.2) and for carbon (C-12) at $Q^2 = 5 \text{ GeV}^2$ (Fig.3) and $Q^2 = 10 \text{ GeV}^2$ (Fig.4) respectively. In the middle panels, the structure functions F_2^A (Eq.(22)), F_L^A (Eq.(23)) and the reduced cross section σ_r^A (Eq.(24)) are shown for lead (Pb-208) carbon (C-12) at $Q^2 = 5 \text{ GeV}^2$ and $Q^2 = 10 \text{ GeV}^2$ in Figs.1-4 respectively. In the right panels, the functions divided by A for the heavy nucleus of Pb-208 and for the light nucleus of C-12 as a function of the momentum fraction x are shown.

We observe that the results are dependent on the impact parameter and the expansion point. The results in these figures (i.e., Figs.1-4) in the first row are dependent on the impact parameter, and they are independent of the expansion point. But in the two and three rows, the results are dependent on those. In the first row, the results increase as the impact parameter increases. The results for the heavy nucleus of Pb-208 are sensitive for different values of $b = 0$ and 5 fm and for the light nucleus of C-12 are dependent on the value of $b = 0$. In the second row, the ratio $R_{F_L}^A$ is dependent on the coefficients a and b . The results for F_L^A and F_L^A/A increase as the impact parameter increases and decreases as the expanding point increases. This is visible as the longitudinal structure function at x is proportional to the gluon density at kx . These upper and lower values are comparable with the original NNPDF3.1 PDF uncertainties [39] as considered in Ref.[40].

In the third row, the ratio $R_{\sigma_r}^A$ is independent of the coefficient a at $b = 0$ and is dependent on it at $b = 5 \text{ fm}$ for $x \leq 10^{-3}$. The increase of $R_{\sigma_r}^A$ towards low x , reflecting the fall of the reduced cross sections (nucleon and nuclei) towards larger y region. This behavior is observable for σ_r^A and σ_r^A/A at low x with increases of the impact parameter and the expansion point for the heavy nucleus of Pb-208 and is visible at $b = 0$ for the light nucleus of C-12. The results increase as the Q^2 values increase in Figs.2 and 4. The importance of the nuclear longitudinal structure function F_L^A at low x in a wide range of the mass number A in all figures is observable as the contribution of F_L^A is enhanced with y^2 and the nuclear reduced cross section σ_r^A tends to $F_2^A - F_L^A$ for $y \rightarrow 1$.

In conclusion, we have discussed the determination of the nuclear reduced cross section and its ratio in the EIC

kinematic range for the heavy and light nucleus Pb-208 and C-12 respectively. The HIJING parametrizations for $R_{F_2}^A$ and R_G^A is used for the nuclear distributions. The nuclear longitudinal DIS structure function $F_L^A(x, Q^2)$ at small x is obtained in terms of the effective parameters of the Froissart-bound parametrization of $F_2(x, Q^2)$ and $R_{F_2}^A$ owing to the expanding point of the gluon density. In the EIC kinematic range, the importance of the longitudinal structure function for nuclei should be required, since the nuclear reduced cross section is dependent on it at high inelasticity. The x dependence of the nuclear longitudinal structure function and nuclear reduced cross section at $Q^2 = 5$ and 10 GeV^2 in a wide range of nuclei have been calculated. The magnitude of these results increases with a decrease of x and an increase of the atomic number A and Q^2 . The results are dependence on the impact parameter of the light and heavy nuclei and the expanding point of the gluon density at small x . The nuclear reduced cross section divided by A has a depletion with increases of y similar to the reduced cross section of the proton in the EIC kinematic range and its dependent on the impact parameter and the expanding point. We hope that this paper can motivate a more accurate determination of F_L^A and σ_r^A in the next years in the EIC colliders.

ACKNOWLEDGMENTS

The authors are thankful to the Razi University for financial support of this project.

TABLE I: The coefficients [5] at low x for $0.15 \text{ GeV}^2 < Q^2 < 3000 \text{ GeV}^2$.

parameters	value
a_{00}	0.255 ± 0.016
a_{01}	$1.475 \times 10^{-1} \pm 3.025 \times 10^{-2}$
a_{10}	$8.205 \times 10^{-4} \pm 4.62 \times 10^{-4}$
a_{11}	$-5.148 \times 10^{-2} \pm 8.19 \times 10^{-3}$
a_{12}	$-4.725 \times 10^{-3} \pm 1.01 \times 10^{-3}$
a_{20}	$2.217 \times 10^{-3} \pm 1.42 \times 10^{-4}$
a_{21}	$1.244 \times 10^{-2} \pm 8.56 \times 10^{-4}$
a_{22}	$5.958 \times 10^{-4} \pm 2.32 \times 10^{-4}$
n	11.49 ± 0.99
λ	2.430 ± 0.153
M^2	$0.753 \pm 0.068 \text{ GeV}^2$
μ^2	$2.82 \pm 0.290 \text{ GeV}^2$
$\chi^2(\text{goodness of fit})$	0.95

REFERENCES

1. J. Aubert et al. (European Muon Collaboration), Phys. Lett.B **123**, 275 (1983).
2. L.S.Moriggi, G.M.Peccini and M.V.T.Machado, Phys.Rev.D **103**, 034025 (2021).
3. Anna M.Stasto, Acta Physica Polonica B **16**, 7-A23 (2023).
4. N.Armento, Eur.Phys.J.C **26**, 35 (2002).
5. M. M. Block, L. Durand and P. Ha, Phys.Rev.D **89**, 094027 (2014).
6. Martin M. Block, Loyal Durand and Douglas W. McKay, Phys.Rev.D **79**, 014031 (2009).
7. M. Froissart, Phys. Rev. **123**, 1053 (1961).
8. L.P. Kaptari, et al., JETP Lett. **109**, 281 (2019).
9. G.R. Boroun, Phys.Rev.C **97**, 015206 (2018).
10. L.P. Kaptari, et al., Phys.Rev.D **99**, 096019 (2019).
11. G.R.Boroun and B.Rezaei, Phys.Lett.B **816**, 136274 (2021).
12. K.J. Eskola, H. Honkanen, V.J. Kolhinen and C.A. Salgado, Phys.Lett.B **532**, 222 (2002).
13. Jamal Jalilian-Marian and Xin-Nian Wang, Phys.Rev. D **63**, 096001 (2001).
14. N. Armento, J. Phys. G **32**, R367 (2006).
15. F. Gelis, E. Iancu, J. Jalilian-Marian, and R. Venugopalan, Annu. Rev. Nucl. Part. Sci. **60**, 463 (2010).
16. R. Abdul Khalek et al., Snowmass 2021 White Paper, arXiv [hep-ph]:2203.13199.
17. R.Abir et al., The case for an EIC Theory Alliance: Theoretical Challenges of the EIC, arXiv [hep-ph]:2305.14572.
18. LHeC Collaboration, FCC-he Study Group, P. Agostini, et al., J. Phys. G, Nucl. Part. Phys. **48**, 110501 (2021).
19. E.Sichtermann, Nucl.Phys.A **956**, 233 (2016).
20. E. C. Aschenauer et al., Phys. Rev. D **96**, 114005 (2017).
21. M. Ericson and S. Kumano, Phys.Rev. C **67**, 022201 (2003).
22. G. Altarelli and G. Martinelli, Phys. Lett. B **76**, 89 (1978).
23. M.B.Gay Ducati and P.B.Goncalves, Phys.Lett.B **390**, 401 (1997).
24. G.R.Boroun and B.Rezaei, Eur.Phys.J.C **72**, 2221 (2012).
25. M. M. Block and L. Durand, arXiv[hep-ph]:0902.0372.
26. G.R.Boroun and B.Rezaei, Phys.Rev.D **105**, 034002 (2022); G.R.Boroun and B.Rezaei, Phys.Rev.C **107**, 025209 (2023).
27. K. J. Eskola, V. J. Kolhinen and C. A. Salgado, Eur. Phys. J. C **9**, 61 (1999).
28. D. de Florian and R. Sassot, Phys. Rev. D **69**, 074028 (2004).

29. M. Hirai, S. Kumano and T. H. Nagai, Phys. Rev. C **76**, 065207 (2007).
30. K. J. Eskola, H. Paukkunen and C. A. Salgado, arXiv[hep-ph]:0802.0139.
31. N. Armesto, J. Phys. G **32**, R367 (2006).
32. E.R. Cazaroto, F. Carvalho, V.P. Goncalves and F.S. Navarra, Phys.Lett.B **669**, 331 (2008).
33. Wei-tian Deng, Xin-Nian Wang and R. Xu, Phys.Lett.B **701**, 133 (2011).
34. [nCTEQ15 Collaboration] K.Kovarik et al., Phys. Rev. D **93**, 085037 (2016).
35. [nNNPDF3.0 Collaboration] R.Abdul Khalek et al., Eur. Phys. J. C **82**, 507 (2022).
36. [EPPS21 Collaboration] K. J. Eskola, P. Paakkinen, H. Paukkunen and C. A. Salgado, Eur. Phys. J. C **82**, 413 (2022).
37. S. -Y. Li and X. -N. Wang, Phys. Lett. B **527**, 85 (2002).
38. W. -T. Deng, X. -N.Wang and R. Xu, Phys.Rev.C **83**, 014915 (2011).
39. NNPDF collaboration, R. D. Ball et al., Nucl. Phys. B **849**, 112 (2011).
40. N.Armesto et al., Phys. Rev. D **105**, 114017 (2023).

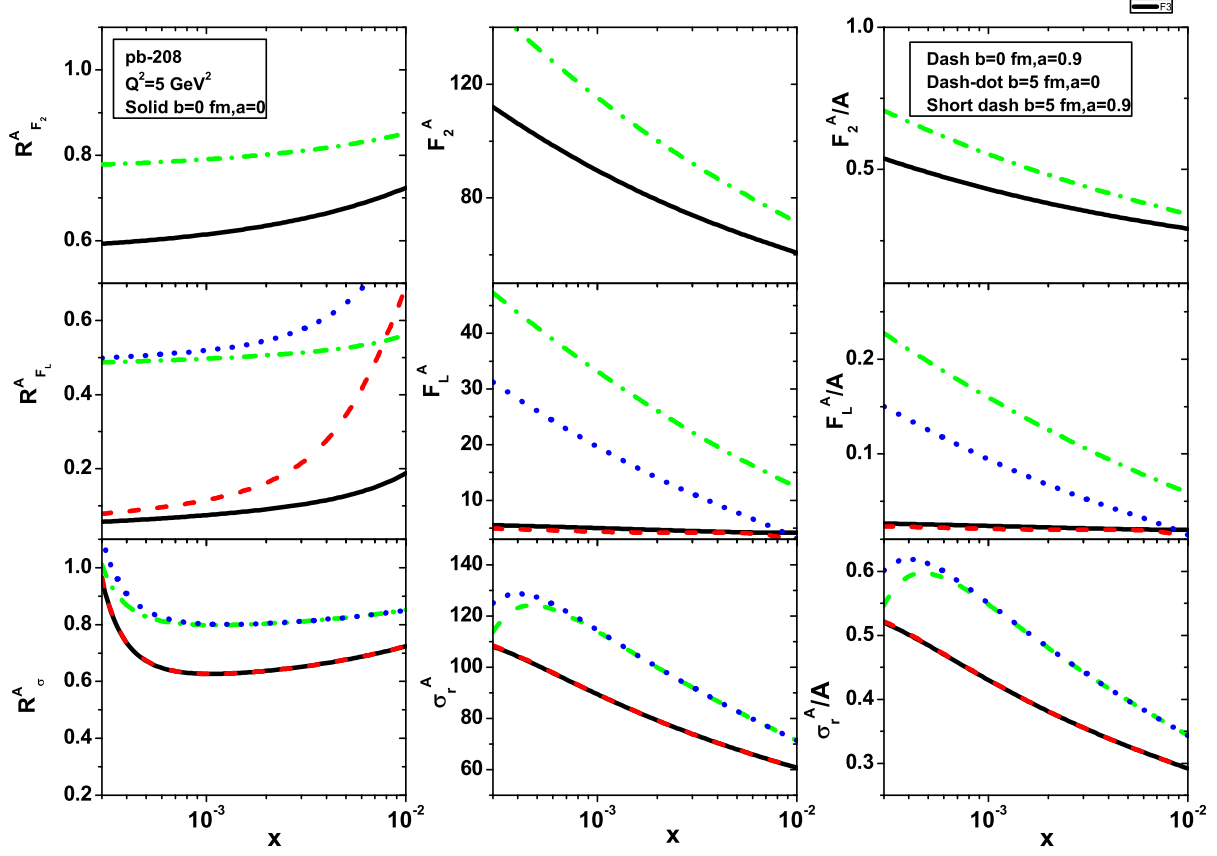


FIG. 1: Results of the ratios, structure functions and reduced cross section of the nucleus of Pb-208 are shown as a function of x at $Q^2 = 5 \text{ GeV}^2$. We observe, in the left panel, the ratios $R_{F_2}^A$, $R_{F_L}^A$ and $R_{\sigma_r}^A$; in the middle panel, F_2^A , F_L^A and σ_r^A ; in the right panel, F_2^A/A , F_L^A/A and σ_r^A/A from up to down respectively. The curves show the results owing to the impact parameters and the expanding points as: $b = 0 \text{ fm}$ and $a = 0$ (solid black), $b = 0 \text{ fm}$ and $a = 0.9$ (dash red), $b = 5 \text{ fm}$ and $a = 0$ (dash-dot green) and $b = 5 \text{ fm}$ and $a = 0.9$ (short dash blue) respectively.

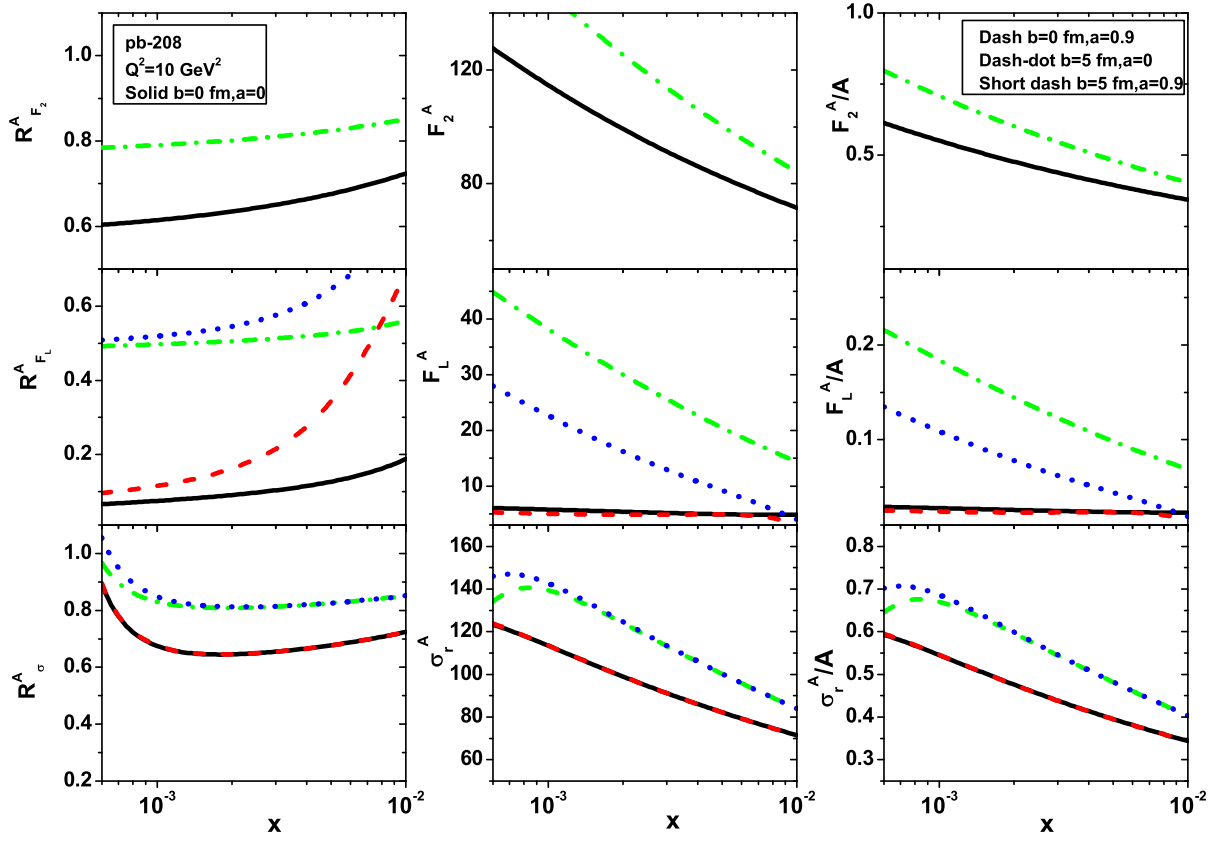


FIG. 2: The same as Fig.1 for the nucleus of Pb-208 at $Q^2 = 10 \text{ GeV}^2$.

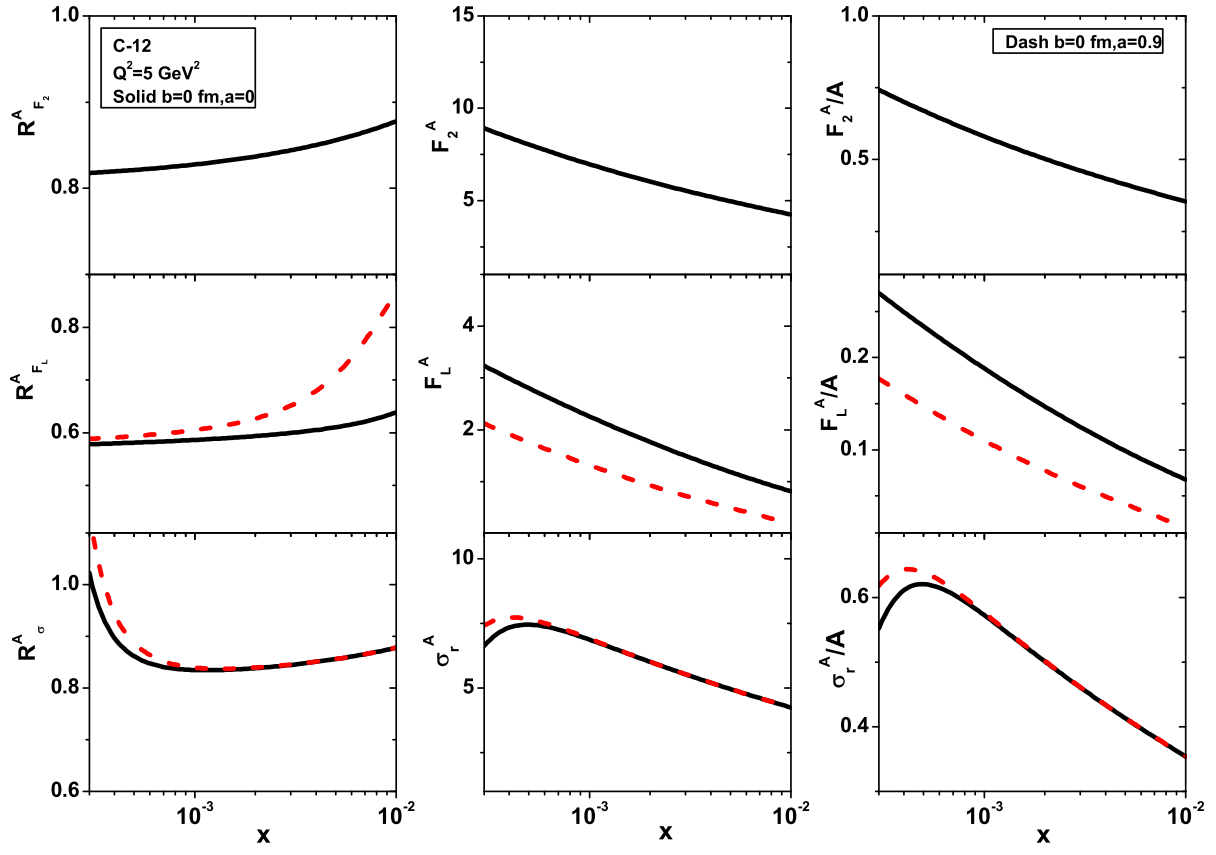


FIG. 3: The same as Fig.1 for the nucleus of C-12 at $Q^2 = 5 \text{ GeV}^2$.

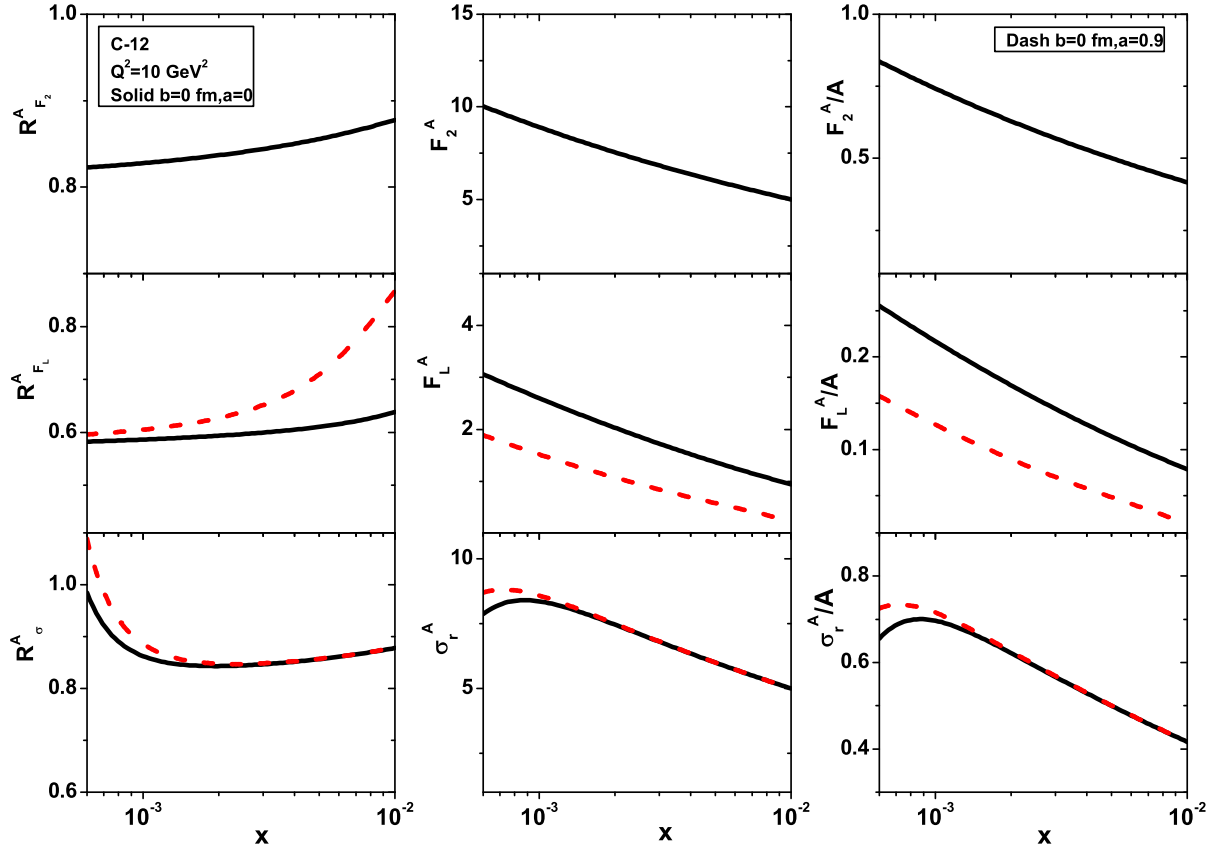


FIG. 4: The same as Fig.1 for the nucleus of C-12 at $Q^2 = 10 \text{ GeV}^2$.